J. Fluid Mech. (2009), *vol.* 638, *pp.* 491–506.
doi:10.1017/S002211200999098X

Heat, salt and momentum transport in a laboratory thermohaline staircase

R. KRISHNAMURTI†

Department of Oceanography and Geophysical Fluid Dynamics Institute, Florida State University, Tallahassee, FL 32306, USA

(Received 17 September 2008; revised 23 June 2009; accepted 28 June 2009; first published online 18 September 2009)

Flow characteristics and fluxes in thermohaline staircases are measured in two tanks differing in aspect ratio A, where A is the ratio of tank width to fluid depth. In one tank (the '1×1' tank) which is 30 cm deep and 30 cm wide, a staircase of one salt-finger layer and one convecting layer develops for a certain setting of the control parameters. The convecting layer has $A \simeq 2$. Shadowgraphs show convecting plumes that appear disorganized, and a large-scale flow never develops. Instead, the finger layer grows in height, overtakes the convecting layer and within a few days becomes one finger layer. The second tank (the '1×5' tank) is also 30 cm deep but is 150 cm wide. For the same control parameter setting a similar staircase with a finger layer 20 cm deep and a convecting layer 10 cm deep develop. The convecting layer, with $A = 15$, has quite a different character. A large-scale flow develops so that the convecting layer has one cell, 10 cm deep and 150 cm wide. In this flow are large plumes which are transient and tilted; particle image velocimetry measurements of Reynolds stresses show they help to maintain the large-scale flow against viscous dissipation. Shadowgraphs show all the finger tips swept in the direction of the large-scale flow adjacent to the finger layer. Measurements show that the large-scale flow 'collects' the salt delivered by the many fingers so that the accumulated negative buoyancy leads to deep convection. This is a more stable arrangement, with the configuration lasting to the order of 10^2 days.

1. Introduction

This is a sequel to an earlier study titled 'Double-diffusive transport in laboratory thermohaline staircases' (Krishnamurti 2003). The basis is to use a fluid whose density ρ is determined by the concentrations of two components which diffuse at different rates. The motivation was to understand ocean processes in which in the subtropics, for example, the upper ocean is stably stratified with hot salty water above cold fresh water. The faster-diffusing temperature T is stabilizing, while the slower-diffusing salinity S is destabilizing. This is the arrangement that can give rise to salt fingers and, in some parameter regime, to a thermohaline 'staircase' wherein layers of salt fingers alternate in the vertical with convecting layers. The latter have vertically well-mixed properties, while the salt-finger layers have a drop in properties across the layer. Hence vertical profiles of T and S have a staircase-like shape (especially as the finger layers have smaller vertical extent than the convecting layers).

† Email address for correspondence: ruby@gfdi.fsu.edu

In the laboratory if flux measurements are involved we prefer not to use temperature, since heat exchange between working fluid and laboratory is hard to control. Instead we use laboratory sugar as a proxy for ocean salt and laboratory salt as a proxy for ocean cold. The diffusivity ratio $\kappa_S/\kappa_T \simeq 10^{-2}$ for salt and heat and is 0.3 for sugar and salt. We will continue to call salty fluid as 'cold' and sugary fluid as 'salty'; κ_T is used to designate the diffusivity of salt and κ_S to designate the diffusivity of sugar.

In the earlier study, the apparatus was built of three segments: the bottom reservoir, the test section and the top reservoir. The fluids in the three segments were separated from each other by a porous membrane which allowed sugar and salt to diffuse through it. The bottom reservoir was filled with 'cold fresh water', i.e. water with no sugar but with salt concentration ΔT. The top reservoir was filled with 'hot salty water', i.e. no salt but with sugar concentration ΔS. The test section was prepared to have a double linear gradient,

$$\left.\begin{aligned} T &= \Delta T(1 - z/H), \\ S &= \Delta S(z/H), \end{aligned}\right\} \tag{1.1}$$

where H is the total height of the test section ($H = 2$ m, 1 m or 0.3 m). All segments had horizontal dimensions 30 cm $\times$ 10 cm.

To summarize the results of this earlier paper, straight salt fingers were seen at the lowest values of ΔS and ΔT, which extended from the bottom reservoir to the top reservoir for all three test sections. At higher ΔS and ΔT (Stern number less than 1; see Krishnamurti 2003), the fingers are lumpy but still extend from the bottom reservoir to the top reservoir. At still higher ΔS and ΔT the flow becomes layered (having a staircase profile in T and S) with alternating finger layers and convecting layers. We still do not have an adequate mapping in parameter space of these various flow forms.

We found also in the earlier work that the salt flux was strongly dependent upon the number n of layers into which the system divided. This varied from 1 to 15 layers in the 2 m tall test section, while ΔS and ΔT were varied by a factor of 2 or 3. With an increase of ΔS by a factor of 2, the flux unexpectedly decreased by as much as an order of magnitude. This was finally rationalized as follows: if $n = 1$, vertically coherent fingers carry down salinity ΔS from the top reservoir in down-going fingers; up-going fingers carry $S = 0$ to the top reservoir; and a certain salt flux is accomplished. However if these fingers are disrupted, say by a convecting layer at mid-depth, then we note that the down-going fingers still leave the top reservoir with ΔS and that the up-going fingers still leave the bottom reservoir with $S = 0$, but these are mixed in the convecting layer approximately to $S \simeq \Delta S/2$. Thus the up-going finger approaching the top reservoir carries salinity that is not zero but $\Delta S/2$. The net effect is that ΔS is exported from the top reservoir but $\Delta S/2$ is returned; the flux is reduced by a factor of two. It is easily shown that with n mixing (convecting) layers the flux is reduced by a factor of $1/(n+1)$. Of course all these different n may not occur for the same ΔS, but the change in ΔS necessary to produce changes in n is small compared to the large (factor $1/(n+1)$) change in flux. Finally, the salt flux across an individual finger layer within the staircase is expressed as

$$N_S \sim R_S^{\gamma} R_{\rho}^{\delta} \tag{1.2}$$

with $\gamma = 0.19$, where N_S is the Nusselt number, the ratio of total salt flux to diffusive salt flux; R_S is the salt Rayleigh number given by

$$R_S = \frac{g\beta\Delta S}{\kappa_T \nu} d^3, \; R_{\rho} = R_T/R_S, \tag{1.3}$$

where g is the acceleration of gravity, β the salt contraction coefficient, κ_T the diffusivity of salt in water, ν the kinematic viscosity and d the salt-finger layer depth. The thermal Rayleigh number R_T is defined below.

The positive value of δ found in our earlier work was unusual, since it might be expected that N_S would decrease with increased R_ρ. However the dependence of N_S on R_ρ might not be monotonic in all parts of the R_S–R_T parameter space, especially in view of the unusual dependence of flux upon n as described above. Also, R_ρ was given a small range (1.1–1.2) in the earlier work.

We may think of the salt-finger layer as bringing down salt and thereby releasing potential energy to drive the convecting layer. Since each finger layer is in balance with its neighbouring convecting layers, and the latter may have its ability to transport salt modified by the closeness of the sidewalls of the tank, we are in the present study investigating the importance of the aspect ratio A of the flow domain. In the earlier work, A for each convecting layer was often of order one, where A is the ratio of tank width to the depth of the layer. In the present study $A \simeq 15$ and the flow form is markedly changed.

In the case of Rayleigh–Bénard convection we have found that a large-scale shearing flow with embedded transient tilted plumes becomes established for Rayleigh number $R_T \gtrsim 2 \times 10^6$, for Prandtl number $Pr = \nu/\kappa_T = 7$ and for $A = 10$–20 (Krishnamurti & Howard 1981). Here

$$R_T = \frac{g\alpha \Delta T}{\kappa_T \nu} d^3, \tag{1.4}$$

where α is the thermal expansion coefficient, ΔT the temperature difference imposed between the bottom and top boundaries and d the fluid depth. The flux law $N_T \sim R_T^\gamma$ has $\gamma = 0.20$ for aspect ratio $A = 12$ and $10^6 \lesssim R_T \lesssim 10^9$ in Krishnamurti (1995). In that paper it was also shown that when the convecting domain originally 120 cm $\times$ 120 cm $\times$ 10 cm was partitioned into 144 cubical domains, each of dimensions 10 cm $\times$ 10 cm $\times$ 10 cm, the exponent was changed to $\gamma = 0.28$ in keeping with other small-A results (Castaign *et al.* 1989). Since R is usually a large number, such a small change in exponent can represent a large change in heat flux. It should be noted that large-A convection has smaller flux than small-A convection.

Thus it is that we built a salt-finger tank with horizontal dimensions 150 cm $\times$ 15 cm. The total depth was 30 cm, but with choice of parameters, the depth of the convecting layer was of the order of 10 cm, for $A \simeq 15$.

2. Apparatus

A schematic diagram of the apparatus (the 1×5 tank) is shown in figure 1. It is basically the same design used by Krishnamurti (2003) except that the horizontal dimensions of the current tank are 150 cm (in x) $\times$ 15 cm (in y), while the old tank (the 1×1 one) was 30 cm $\times$ 10 cm. As in the earlier design the tank consists of three segments: the bottom reservoir, the test section and the top reservoir. Porous membranes separate the three segments. These are Versapor 800 membranes (0.8 micron pore size) of 154 cm $\times$ 19 cm $\times$ 0.01 cm, each stretched taut and held in place in an O-ring groove. The bottom and top reservoirs are each 18 cm deep, and each has a capacity of 40 L. The test section is 30 cm deep, and the working fluid occupies 70 L. The Plexiglas walls are 1.9 cm thick.

Each reservoir had four Teflon-coated magnetic stirring bars mounted on an acrylic cradle attached to a shaft that was free to rotate. The stirring bar was driven from outside the tank by another magnetic bar, which was driven by a 4 W synchronous motor at 60 r.p.m.

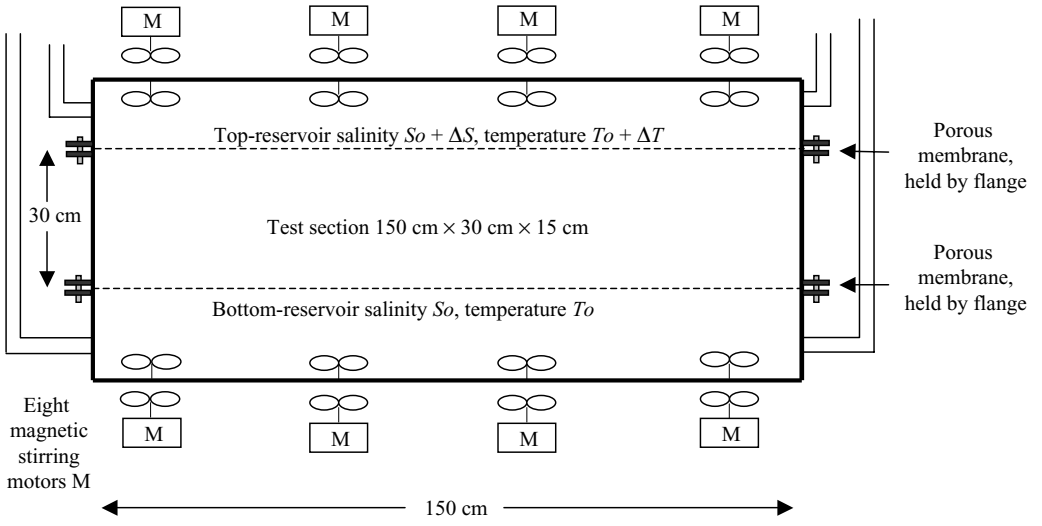

FIGURE 1. Schematic diagram of apparatus (1 × 5 tank).

The three segments of the tank were assembled as follows. There was a flange made of 2.54 cm thick Plexiglas on each reservoir and a matching flange on the top and bottom of the test section. The flange had two O-ring grooves and 68 boltholes. After the bottom reservoir was filled with the desired fluid the porous membrane was stretched over this fluid and held taut by means of an O-ring which fitted in a groove in the Plexiglas flange. Care was taken to allow no air bubbles to be trapped under the membrane. In this tautly stretched state, the membrane was flat and rigid. Stirring the fluid on one side of it did not induce flow on the other side. The membrane allowed salt and sugar to diffuse through it in accordance with the concentration gradient across it. Fluid flow could be forced through it, but we always took precautions in these experiments to ensure that this would not happen. Thus when fluid was to be extracted from the bottom reservoir, the top reservoir lines were closed. Likewise, for extracting fluid from the top reservoir the bottom lines were closed. With the membrane tautly in place, another O-ring was set in its groove in the flange (just outside the one holding the membrane). The function of this O-ring was to provide the seal when the two matching flanges were bolted together with 68 bolts.

Now with the test section in place, it could be filled by the procedure described below. Then another stretched Versapor filter was placed on top of this fluid, held tautly in place by another O-ring in its groove; the sealer O ring was set in place; the top reservoir was placed over this; and the two flanges were bolted together with a further 68 bolts.

The reservoirs are not maintained at fixed S and T but are allowed to decay from their initial settings. With reservoir depths comparable to working fluid depth, the decay rate is small enough for the working fluid to respond nearly quasi-statically. The rundown generally takes several months. The eight motors turning the stirring magnets in the reservoirs run continuously for the duration of the experiment. Sodium fluoride in all solutions was essential to prevent microbial growth for such a long experiment.

The whole apparatus is housed in a light-tight blackbox 185 cm × 244 cm × 200 cm and was climate controlled by an external unit.

To obtain shadowgraphs, photographic paper 28 cm (in z) $\times$ 2 m (in x) was attached in the dark to a rigid target usually kept 40 cm from the tank. (On some occasions, the paper was attached directly to the tank.) A 2 W zirconium arc lamp with arc diameter 1 mm acted as a 'point source'. It was usually located 1 m from the front surface of the tank. Thus magnification of the image on the paper was small and could be easily calculated. Exposure times were usually around 20 s.

For particle image velocimetry (PIV) the working fluid was seeded with silver-coated hollow glass spheres, with diameter 10–30 microns. These had been separated in a settling experiment to select those which were nearly neutrally buoyant at the mean density (mid-depth density) of the working fluid. A 25 mW laser light sheet, spread by a cylindrical lens, was reflected into the tank to illuminate a sheet of fluid mid-distance in y. A 4 megapixel digital camera was used to obtain sequential photographs of the tracer particles.

For flux measurements we used a specific gravity balance to determine its specific gravity to four decimal places and an immersion-type conductivity probe to determine salinity of the reservoir fluids at fixed time intervals.

3. Procedure

First, the 1×5 tank was levelled to $\pm 10^{-4}$ radians.

We used the values of R_S and R_T which we learned had produced one finger layer and one convection layer ($n = 2$) in the 30 cm wide, 30 cm deep tank. The bottom reservoir was filled with salt solution (representing 'cold fresh' water) of concentration 14.2 g per litre; the top reservoir with sugar solution of concentration 21.3 g per litre. In several trials we varied these concentrations only a little.

The test section was filled with opposing gradients of sugar and salt, starting at the bottom with no sugar and salt matching that in the bottom reservoir, and ending at the top with no salt and sugar matching the concentration of the top reservoir. This was accomplished using the two-bucket method (Oster 1965) but with a modification on delivery. Two identically sized holding barrels, one for sugar solution, the other for salt solution, were placed high above the test section, with the salt tank containing a magnetic stirring bar and placed upon a motor-driven magnetic mixer. The two holding tanks were connected with a siphon so that their fluid heights would remain equal. The salt solution was then gravity fed into the test section through eight 1 mm diameter hypodermic tubes of equal lengths on to eight floating sponges. This was to distribute fluid and minimize horizontal gradients. Since this would lead to sugar solution siphoning into the salt-holding tank, the later was constantly stirred with the magnetic stirring bar. As the sugar solution was less dense than the salt solution, the later-entering fluid would lie above earlier-entering fluid in the test section. The flow rate was slowed to produce a filling rate of 1 cm depth per hour. At this rate it takes approximately 30 h to fill the test section. Also at this rate, early formed fingers or other flow structures showed no visible disruption.

When the test-section filling was completed, the top porous membrane was stretched into place and the top reservoir bolted on. Then the top reservoir was filled with the sugar solution. Throughout the duration of the experiment, the reservoir stirring was maintained.

In this rundown mode, fluid samples were extracted from the reservoirs at fixed time intervals, conductivity c and density ρ measured (from which T and S could be deduced); then the samples returned to the reservoirs with very little loss of volume. The conductivity metre was calibrated against standards with every data taking. We

used the following procedure for fluid extraction. With the lines to the lower reservoir closed, the upper reservoir was opened and 50 mL of well-mixed fluid was extracted. After measurement of c and ρ and return of the sample to the upper reservoir, the upper reservoir was then sealed. Then the two lines to the lower reservoir were opened, and 50 mL of well-mixed fluid were extracted from one end of the tank by adding 50 mL of the previous day's extraction to the other end. We note that the error introduced when 50 mL of slightly differing properties (about 0.1 %) was mixed into 40 L was smaller than our measuring error. The flux was determined by the change in property in the reservoir with time, as was done by Schmitt (1979).

Early in the experiment data was collected twice per day. As the decay rate decreased, data was collected once per day. Thus, once per day the reservoir fluids were analysed. Also once per day, a shadowgraph photo was exposed, followed immediately by a vertical scanning to determine the optical rotation angle $\theta(x)$. A series of calibration measurements was made so that from any pair of measurements (c, ρ) the salt and sugar concentrations could be determined. For the internal measurements of $\theta(x)$ the equations of Ruddick & Shirtcliffe (1979) were used to infer the sugar concentration $w_S(z)$ while using a mean value of salt concentration appropriate for that depth. PIV was done extensively to find the relationship between the flows and the shadowgraph images.

4. Observations

4.1. *Shadowgraphs*

Figure 2(a) shows a typical example of a shadowgraph showing the density structure in the wide tank. It represents 124 cm $\times$ 21 cm taken out of an original photograph 185 cm (in x) $\times$ 28 cm (in z). The intention was to show the horizontal uniformity of the flow which is a staircase of only one step: one finger layer and one convection layer (labelled $n = 2$, where n signifies the number of layers). In this example the fingers are approximately 20 cm deep and lie above the convecting layer which is approximately 10 cm deep. This configuration persists for about 10^2 days.

Fingers show well in shadowgraph apparently because of large contrasts in refraction index. The convecting layer being better mixed appears to be uniform, but its flow structure will be revealed below by means of PIV. The nearly vertical fingers appear to end in a zigzag or reverse-S shape with their ends apparently swept away to the right. Figure 2(b) shows an enlargement of this aspect of the flow. Figure 3(a) shows a similar enlargement at lower ΔS than in figure 2(b), with a well-developed large-scale flow in the convecting layer.

The convecting layer was observed to have, initially, a high flux and high Nusselt number and as many as eight cells (labelled $m = 8$). This is in a 10 cm deep, 150 cm wide domain occupied by the convecting layer. One of the sinking regions separating two cells when $m = 3$ is shown in figure 3(b). As the experiment progressed with ΔS, ΔT and N_S gradually decaying from initial values, the number of convecting cells decreased from eight to ultimately one ($m = 1$). This is the state shown in figure 2(a).

By contrast, the convecting layer in the small tank (the 1×1 one) is shown in figure 4. It occupies a domain 19 cm deep, 30 cm wide. The transient plumes or buoyant elements were never organized into a large-scale flow. Instead the finger layers extended, and the convecting layer shrank and vanished within a few days.

(*a*)

(*b*)

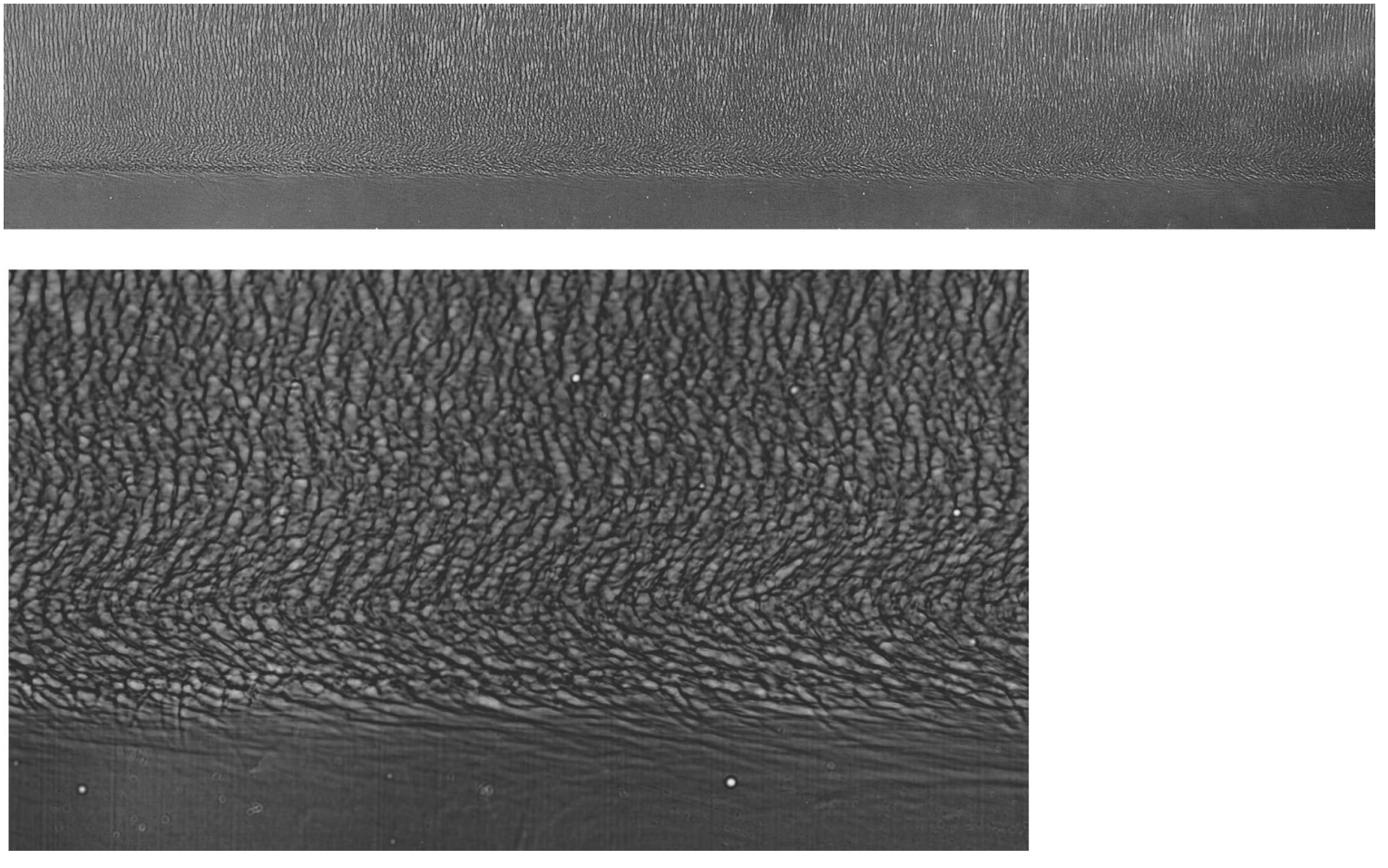

FIGURE 2. (*a*) Shadowgraph showing one finger layer and one convecting layer ($n = 2$) with one cell ($m = 1$) in the convecting layer. It shows 100 cm out of the total 150 cm width in x (1×5 tank). (*b*) Shadowgraph of salt fingers above a convecting layer, with large-scale flow from left to right directly under the fingers. The image represents 9.2 cm in the x direction and 5.2 cm in the z direction and is excerpted from a photograph 150 cm wide and 30 cm tall, which was uniformly of this character at all x as shown in (*a*). The fingers occupied 20 cm, and the convection occupied 10 cm in depth. Note the tilt of the fingers that end in the convecting flow (1×5 tank).

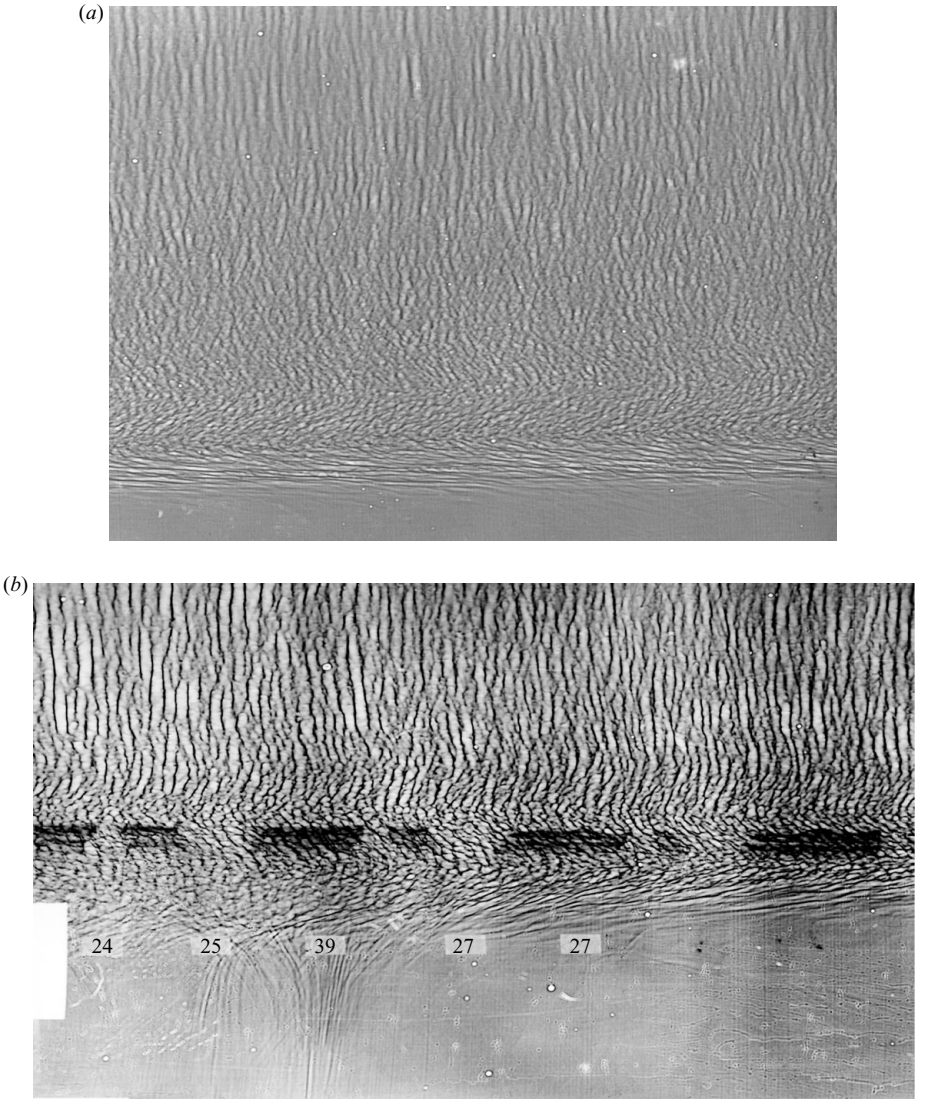

FIGURE 3. (*a*) Shadowgraph of a portion of case $n = 2$, $m = 1$ showing fingertips swept away in a well-developed shear flow (1×5 tank). (*b*) Shadowgraph of a portion of case $n = 2$, $m = 3$ showing the downwelling plume in refractive index and in optical rotation. The numbers superposed on the photograph are rotation angles and indicate the high sugar concentration in the downwelling plume as well as the horizontal sweeping effect of the flow into the plume (1×5 tank).

4.2. *Particle image velocimetry (PIV)*

Ten millilitres of sugar solution containing the selected tracer particles were introduced into 70 L of working fluid from the upper left side of the tank. After this initial disturbance, the fingers are seen to be healed in figure 5(*a*), 5 h after injection. Here a sheet of green laser light illuminates the particles at mid-distance (in y) between the two walls. The down-going finger flow has apparently carried particles down into the convecting layer below (seen in figure 5*b*) in which there is a rightward flow near

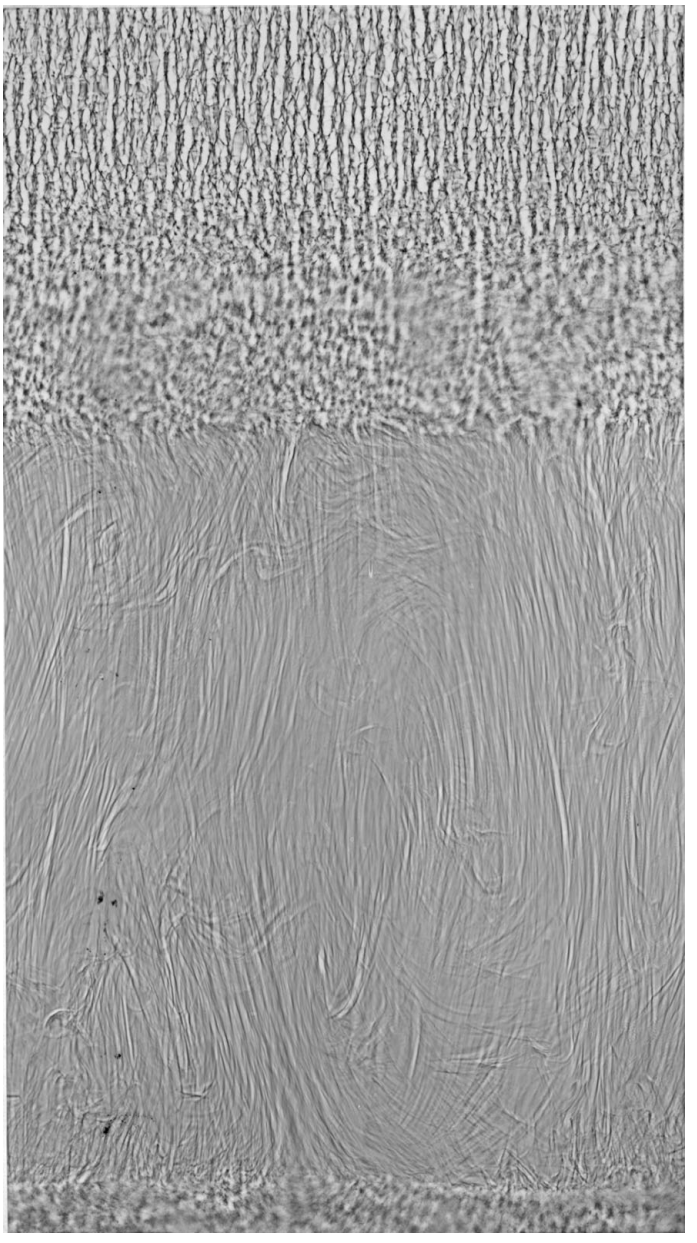

FIGURE 4. An unorganized convection layer in the 1×1 tank.

the top as seen by the green and a leftward flow near the bottom of the layer in which particle-free (dark) fluid has come from the lower right end of the tank. Transient plumes such as the one captured in figure 5(*b*) appear to tilt from the lower left to the upper right. It thus appears that rising fluid moves up and to the right, carrying rightward momentum upward to where the flow is already rightward, and sinking fluid moves down and to the left, carrying leftward momentum to where the flow is leftward.

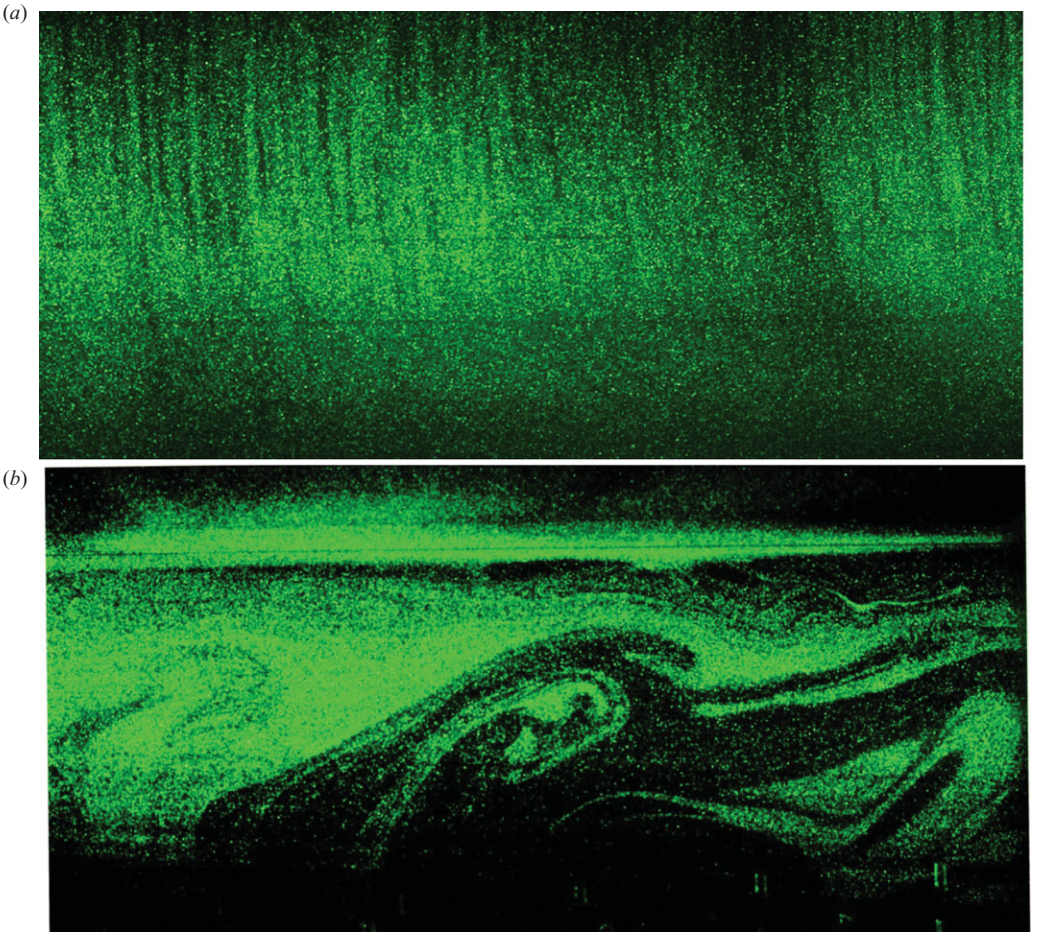

FIGURE 5. Tracer particles in a vertical sheet (x, z) at mid-depth in y, showing (a) fingers in the upper part of the tank and (b) tilted plumes in a large-scale shearing convection in the lower part of the tank. The tracers were introduced from the upper left, 5 h prior to this imaging. They travelled downward in the down-going fingers and entered the convecting fluid. Meanwhile fluid free of tracers came from the far right along the lower part of the convecting layer, leading to this visualization. Both (a) and (b) represent approximately 10 cm in z and 22 cm in x out of the total horizontal dimension of 150 cm.

To check this, PIV Sleuth (Christiansen, Soloff & Adrian 2001) was used to obtain the velocity field in the x–z plane. An example is shown in figure 6, with mean flow $\langle u \rangle$ and Reynolds stress $\langle uw \rangle$ (where the brackets refer to local horizontal average) shown in figures 7(a) and 7(b). Between $z = 60$ and $z = 90$ where $\langle uw \rangle$ is positive, the tilted plumes do indeed carry rightward (leftwards) horizontal momentum upward (downward). Here $\langle uw \rangle$ and $(\mathrm{d}/\mathrm{d}z)\langle u \rangle$ have the same sign indicating that the kinetic energy of the mean flow increases at the expense of the fluctuating flow (Krishnamurti 2005). To obtain a more global view, instantaneous images of the whole 150 cm $\times$ 10 cm domain would have been desirable. However, for high resolution and to avoid refractive-index-induced errors, we viewed only 8 cm $\times$ 10 cm domains at narrow angles so that all points on this domain were viewed nearly normal to the tank wall.

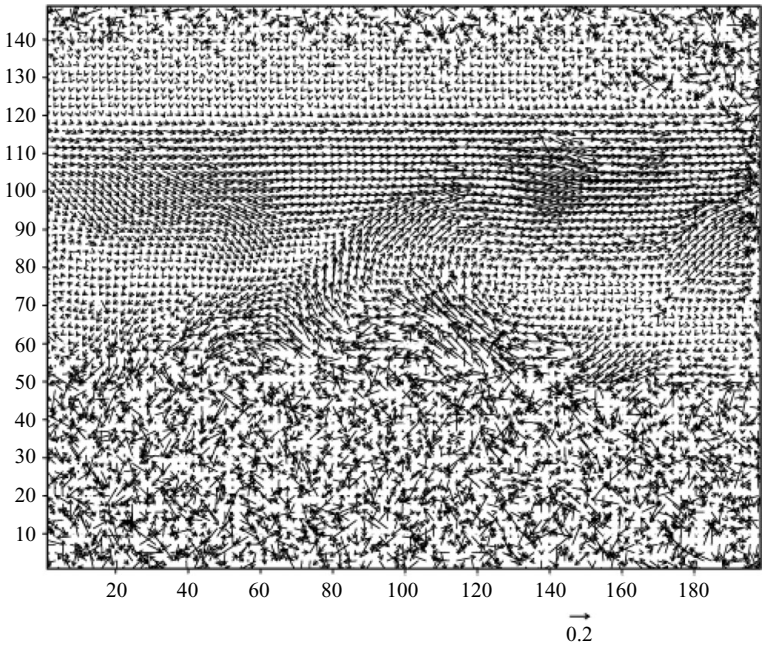

FIGURE 6. (*a*) A portion of the PIV-derived flow vectors on the vertical (x, z) sheet, as in figure 5.

Repetitions in time were composited and are shown in figure 8. These are for repeating transient plumes; equal time has not been given to quiescent periods without plumes.

Of course the swept appearance of fingertips suggesting a large-scale flow in the convection layer was seen in the shadowgraphs of many runs before PIV tracers were introduced. Also the reverse-*S* shape seen just above the fingertips may be a reaction to fluid being stressed to the right. Similar behaviour is seen in confined flows even without double diffusion.

4.3. *Flux measurements*

The salt flux, expressed non-dimensionally as Nusselt number N_T, is shown plotted against the Rayleigh number R_T in figure 9. The flux curves are labelled not only by the tank aspect ratio (1×5 or 1×1) but also by the number (n) of layers in the vertical and the number (m) of cells in the horizontal within the convecting layer. Of note are the higher Nusselt numbers for the 1×5 tank than for the 1×1 tank, for the range $R_T = 5 \times 10^{12}$ to 7×10^{12} in which overlapping data exists. This observation needs careful interpretation to avoid misleading.

The Nusselt number is the total flux F_T divided by the diffusive flux $\kappa_T \Delta T/d$. However, in a 'rundown' experiment, ΔT at any given time is not prescribed but rather is the result of the flux that has preceded. For a slow decay (through quasi-static states) the Nusselt number is a useful measure of non-dimensionalized flux. However, in comparing the two experiments, the 1×5 tank appears to have larger N_T than the 1×1 tank. We observed that in the 1×5 tank, the flux was generally smaller at comparable R_T (in keeping with the smaller flux when a large-scale flow is established as in Rayleigh–Bénard convection), but ΔT had fallen more quickly from its initial value than in the 1×1 tank, leading to the larger N_T and smaller R_T at early time.

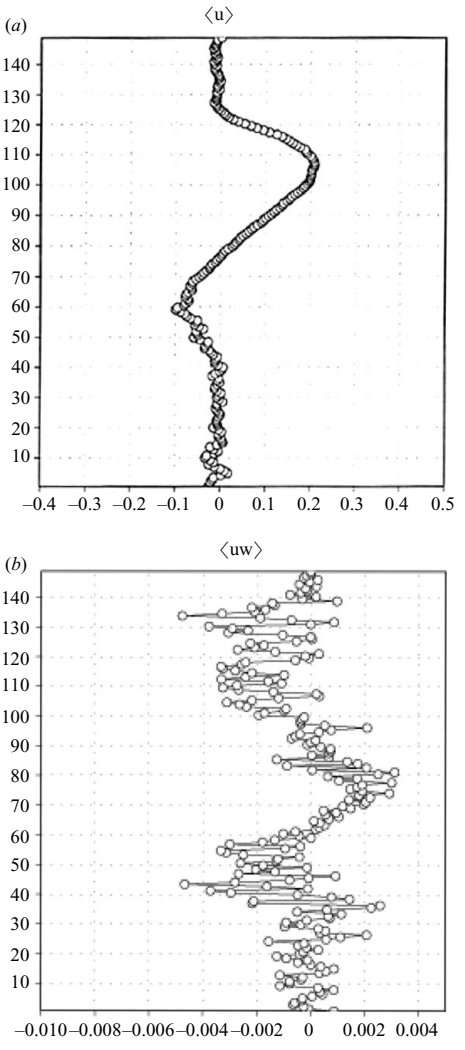

FIGURE 7. (*a, b*) Analysis of the flow vectors of figure 6. The first graph (*a*) shows the horizontally averaged horizontal component of velocity $\langle u \rangle$ as it varies with vertical coordinate z. The second (*b*) shows the horizontally averaged Reynolds stress $\langle uw \rangle$ as it varies with z. Positive $\langle uw \rangle$ where $\partial \langle u \rangle / \partial z$ is also positive (between $z = 60$ and $z = 90$) indicates that the kinetic energy of the mean flow $\langle u \rangle$ increases at the expense of the kinetic energy of the fluctuating flow.

The comparison of the fluxes at comparable times is only approximate. Time $t = 0$ is set for both tanks at the hour when the top reservoir is fixed and filled. However the two filling rates of the test section are not identical. Furthermore the 1×1 tank has reservoirs twice the depth of the 1×5 tank so that decay rates for the 1×1 tank should be smaller. Nevertheless, it is a clear result that the two-layer staircase lasts only 5 days in the 1×1 tank but over 100 days in the 1×5 tank.

We also note that in the 1×1 tank the rundown from two initial points ($R_T = 9.3 \times 10^{12}$, $N_T = 53$) and ($R_T = 8.4 \times 10^{12}$, $N_T = 54$), each with four layers ($n = 4$), takes the system along two different paths for several days (one data point per day is shown), until the two curves appear to asymptote when $n = 1$. This portion of the

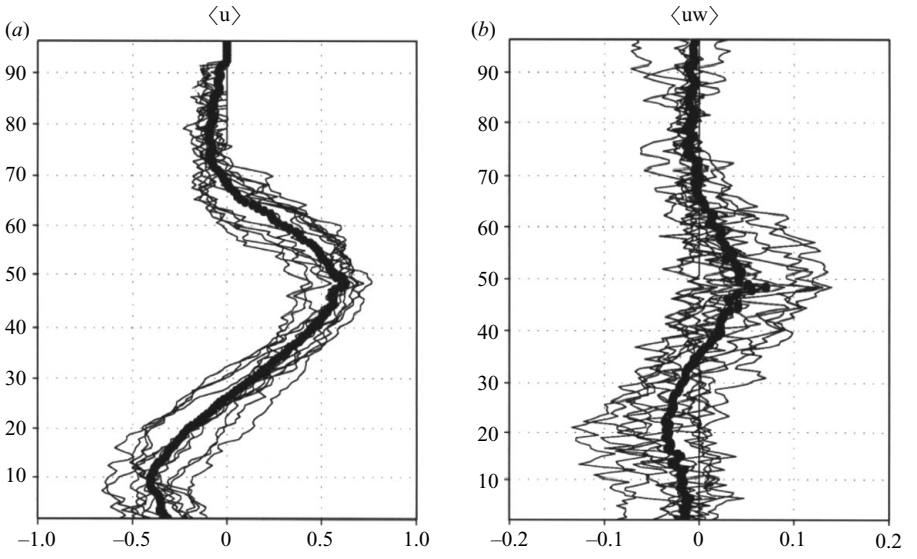

FIGURE 8. Composited $\langle u \rangle$ and $\langle uw \rangle$ for 10 separate plume passages past a stationary camera. To composite, the height z was adjusted so that the maximum $\langle u \rangle$ was placed at the same height.

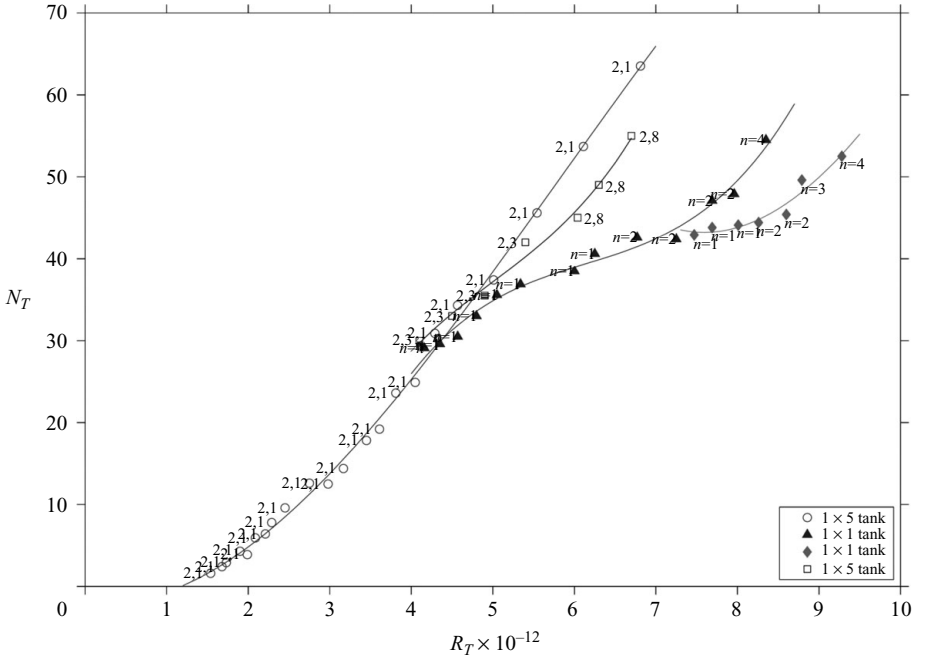

FIGURE 9. Nusselt number N_T versus Rayleigh number R_T for the 1×5 and 1×1 tanks. For the 1×5 tank, the pair of digits by each data point refers to the number of layers n and the number of cells m within the convecting layer. For the 1×1 tank, m was not defined, and only the value of n is given. The measurement error is less than the size of the data points.

curve, with $n = 1$, has the smallest slope, while higher n has steeper slopes. We observe that the shape of the four curves depends most strongly on the number of layers n.

The sugar fluxes F_S for the 1×5 tank were less well measured than the salt fluxes F_T. The changes in specific gravity of the bottom reservoir after 30 days are easily seen, as it changed from 1.0370 to $1.0400 \pm (1 \times 10^{-4})$ in that time. The changes daily measured averaged an increase of 1.0×10^{-4} with a standard deviation of $\pm 1.4 \times 10^{-4}$. The approach is very noisy. This is in part due to instrument limitations. The measurement precision is $\pm 0.5 \times 10^{-4}$, but care is needed for temperature correction of the sample, for temperature equilibration of sample to instrument and in reproducing the same shape of meniscus of the free surface. A more representative measure of precision might be $\pm 1.0 \times 10^{-4}$, and changes in specific gravity should be measured after longer time intervals than one day.

As a typical example, a 30-day accumulated increase in specific gravity of the bottom reservoir was $(19 \pm 1) \times 10^{-4}$. For the same period the density loss from the upward salt flux was

$$\alpha F_T = (53.2 \pm 0.1) \times 10^{-4}. \tag{4.1}$$

Thus the inferred sugar flux downward was

$$\beta F_S = (72.2 \pm 1) \times 10^{-4}, \tag{4.2}$$

leading to a flux ratio

$$F_R = \alpha F_T / \beta F_S = 0.74 \pm 0.02, \tag{4.3}$$

where R_ρ varied from 1.13 to 1.20. This is in agreement with the range of values observed by previous authors (Lambert & Demenkow 1972) but smaller than the value $F_R = 0.88$ for $R_\rho = 2$ obtained by Griffiths & Ruddick (1980).

The density ratio $R_\rho = \alpha \Delta T / \beta \Delta S$ during this 30-day period changed from an initial $R_\rho = 1.13$ to $R_\rho = 1.32$. This amounts to a small (1 %) change in flux, since F_T depends weakly on R_ρ as $R_\rho^{-\gamma}$ with $\gamma = 1/12$ (see for example Lambert & Demenkow 1972). We noticed that the increase in density of the bottom reservoir was larger than the corresponding decrease for the top reservoir; there must have been reorganization of the initial linear profile of the interior. The downward mass flux is not purely from the top reservoir but is mass removed from the upper layers as well.

4.4. *Optical rotation measurements*

The laser beam penetrated the fluid in the y direction and reflected back through the fluid along nearly the same path (at a small angular difference), and the analyzer angle for minimum intensity was recorded. This system was used to scan the fluid in the x direction for each constant height z. Some of the recorded angles are shown in the shadowgraphs.

For example, in figure 3(b), angles in the vicinity of a sinking plume clearly show higher values of optical rotation than neighbouring points. The main point is that with $n = 2$ and $m = 1$, the measurements along z_0 just below the height at which the fingertips in the shadowgraph are swept away, the angles progress from 22 ± 2 div at the left end of the tank to 52 ± 2 div where 1 div $= 0.44°$ at the right end at which sinking begins. As expected, the large-scale flow just under the fingertips becomes progressively more laden with sugar.

5. Discussion

If a large-scale flow becomes established in the convecting layer, then it follows that a large-scale horizontal gradient of property (T or S) will also become established.

The flux of 'salt', $\boldsymbol{F_S}$, can be written as $\boldsymbol{F}_S = \boldsymbol{F}_S^v\hat{\boldsymbol{k}} + \boldsymbol{F}_S^h\hat{\boldsymbol{i}}$ where $\hat{\boldsymbol{i}}$ and $\hat{\boldsymbol{k}}$ are unit vectors in the horizontal (x) direction and the vertical (z) direction respectively; $\boldsymbol{F}_S^v$ is the quantity usually measured in salt-finger experiments and is expressed in terms of $(\Delta S_v)^\gamma$ the imposed vertical salinity difference to some exponent γ.

The large-scale flow (here left to right at the top of the convecting layer and adjacent to the bottom of the finger layer) advects the small 'salt' anomalies δS delivered by each down-going finger until it has collected $\sum \delta S \simeq L\delta S$, where L is the tank width and the sum is apparently large enough to overcome the overall stable stratification and to produce deep convection. With this deep convection at the right endwall the horizontal flux F_s^h has been converted to a vertical flux and is collected in the bottom reservoir as if it had been a vertical flux. In a higher-Nusselt-number regime, sweeping a distance less than L appears to be sufficient to overcome the stable stratification, and the observed flow in the convecting layer has $m > 1$.

One is reminded of the fixed flux case of Rayleigh–Bénard convection in which the temperature gradient rather than the temperature is fixed at the boundaries. In that case the critical Rayleigh number R_c for onset of convection is $R_c = 5!$ with critical wavenumber $a_c = 0$. At onset, cells are infinitely wide, rather than comparable to the layer depth for fixed temperature boundary conditions. The flow at onset travels along the bottom (top) becoming ever hotter (colder) as it travels, unlike the fixed-T case. But of course in the present experiments the Rayleigh number is of the order $10^9\ \Delta T$, which is probably far above onset conditions.

The number of layers n in a finite-depth domain corresponds to the layer height h_i in an unbounded domain. The Nusselt number has been shown (Krishnamurti 2003 and the present study) to have a strong dependence on n, and what determines n is clearly an important question. We have not been able to address this issue in the present study, having fit only one finger layer and one convecting layer into the domain.

What we have shown is the internal dynamics of how convection is maintained in a staircase, and we have shown the importance of large aspect ratio for this dynamics to hold.

In previous experiments with small aspect ratio the convecting layer would be annihilated by finger layers. Mergers of pairs of expanding finger layers were not simultaneous for all pairs, leading to an inhomogeneously layered system which continued to evolve. This was not conducive to the study of control of layer depths.

Now, having seen that a large aspect ratio convecting layer with large-scale flow is stable against expanding finger layers, it seems possible to proceed, for example, with a laboratory-based critique of the model of staircase formation of Radko (2005).

Finally, when there are external sources of horizontal momentum (other than the 'internal' source $\partial\overline{(u'w')}/\partial z$ due to the reorganization of convection itself) it would seem apparent that the latter (internal source) could be of small importance. This present study is not about externally forced horizontal momentum but about a self-generated horizontal shear flow and about measuring vertical flux of horizontal momentum in such a flow.

6. Summary and conclusions

Starting with the same initial conditions, both the '1×5' and the '1×1' tanks developed a staircase with one finger layer and one convecting layer ($1f$, $1c$). The 1×5 convecting layer (with aspect ratio $A \simeq 15$) developed a large-scale flow, but the 1×1 (with $A \simeq 2$) did not. In the 1×5 tank, the finger layer was 20 cm deep and the convecting layer 10 cm deep. This configuration lasted for order-10^2 days even as

the system decayed. The 1×1 tank had larger flux and larger Rayleigh number (and smaller Nusselt number) compared to the 1×5 tank at comparable early time, but within a few days the finger layer in the 1×1 tank overtook the convection layer, leaving only one finger layer thereafter.

This large-scale flow on the convecting layer is maintained in part by the Reynolds stress divergence, as in the Rayleigh–Bénard convection. In the staircase it has the additional feature of collecting the 'salt' delivered by the 'salt fingers' and thereby maintaining a deep convection.

In ocean occurrence, horizontal dimensions are generally large compared to depth, and it would appear that the aspect ratio of convecting layers in thermohaline staircases may be quite large. The results of flow at small A created by laboratory walls may not be applicable. This study shows the stabilizing (long-lasting) nature of large-A convection and in fact may be important for staircase maintenance.

I am grateful to Professor Ron Adrian for making available the data analysis program PIV Sleuth and to T. N. Krishnamurti and his staff for help with computing problems. This research was supported in part by the National Science Foundation under grant number OCE-0242535. This is contribution number 461 of the Geophysical Fluid Dynamics Institute at Florida State University.

REFERENCES

Castaign, B. Gunrantne, G., Heslot, F., Kadanoff, L., Libchaber, A., Thomae, S., Wu, X.-Z., Zaleski, S. & Zanetti, G. 1989 Scaling of hard thermal turbulence in Rayleigh–Bénard convection. *J. Fluid Mech.* **204**, 1–30.

Christiansen, K. T., Soloff, S. M. & Adrian, R. J. 2001 PIV Sleuth: integrated particle image velocimetry (PIV) interrogation/validation software. *Tech Rep.* 943. Department of Theoretical and Applied Mechanics, University of Illinois at Urbana-Champaign.

Griffiths, R. W. & Ruddick, B. R. 1980 Accurate fluxes across a salt-sugar finger interface deduced from direct density measurements. *J. Fluid Mech.* **99**, 85–95.

Krishnamurti, R. 2005 Double-diffusive interleaving on horizontal gradients. *J. Fluid Mech.* **558**, 113–131.

Krishnamurti, R. 2003 Double-diffusive transport in laboratory thermohaline staircases. *J.Fluid Mech.* **483**, 287–314.

Krishnamurti, R. 1995 Low-frequency oscillations in turbulent Rayleigh–Bénard convection: laboratory experiments. *Fluid Dyn. Res.* **16**, 87–108.

Krishnamurti, R. & Howard, L. N. 1981 Large-scale flow generation in turbulent convection. *Proc. Natl Acad. Sci.* **78**, 1981–1985.

Lambert, R. B. & Demenkow, J. W. 1972 On the vertical transport due to fingers in double-diffusive convection. *J. Fluid Mech.* **54**, 627–640.

Oster, G. 1965 Density gradients. *Scient. Am.* **213**, 70–76.

Radko, T. 2005 What determines the thickness of layers in a thermohaline staircase? *J. Fluid Mech.* **253**, 79–98.

Ruddick, B. R. & Shirtcliffe, T. G. L. 1979 Data for double-diffusers: Physical properties of aqueous salt-sugar solutions. *Deep-Sea Res.* **26A**, 775–7873.

Schmitt, R. W. 1979 Flux measurements at an interface. *J. Mar. Res.* **37**, 419–436.